Comparative Experiments with MAPS on Different Parameterization Schemes for Surface Moisture Flux and Boundary-Layer Processes

ZAITAO PAN,* STANLEY G. BENJAMIN, JOHN M. BROWN, AND TATIANA SMIRNOVA**

NOAA/ERL Forecast Systems Laboratory, Boulder, Colorado

(Manuscript received 5 February 1993, in final form 21 July 1993)

ABSTRACT

This study compares several formulations parameterizing the surface moisture flux and boundary-layer processes using the $\theta-\sigma$ hybrid-b model of the Mesoscale Analysis and Prediction System (MAPS) within both 1D and 3D frameworks.

A modified formula for computing the surface moisture flux is proposed based on the assumption that the layer below the lowest model computational level can be represented by three "physical" layers, of which the bottom one is the molecular layer. This three-layer aerodynamic (3LAD) scheme is compared with two-layer aerodynamic (2LAD) as well as flux matching and Penman–Monteith potential evapotranspiration (PM) schemes. Both a 10-day forecast period (3D) and case simulations demonstrate that the 3LAD scheme gives the best prediction in latent heat flux from the ground and mixing ratio in the atmosphere. The moisture flux produced by the 2LAD scheme is too large, especially over warm and moist surfaces. The mean 12-h forecast rms errors in relative humidity at the surface (10 m AGL) are 15.6%, 21.5%, and 26.0%, respectively, for the 3LAD, PM, and 2LAD schemes in a 10-day parallel test period using MAPS.

For the boundary-layer parameterization, the Mellor–Yamada level 2.0 turbulence scheme (MY) and Blackadar convective scheme are compared. Results show that the MY scheme gives more reasonable boundary-layer structure and smaller rms forecast errors.

1. Introduction

For many years, evidence has accumulated from both climate and model forecast experiments showing that atmospheric models are sensitive to both boundary-layer physics and surface processes (e.g., Deardorff 1972; Charney et al. 1977). Many studies (e.g., Miyakoda and Sirutis 1977; Mesinger and Lobocki 1991) have examined the effects of different kinds of surface processes and boundary-layer parameterization schemes. However, the majority of these studies were limited to shallow boundary-layer models or to 1D models. Few tests have been made in fully 3D models extending throughout the whole troposphere to include the interactions between the boundary-layer processes and free atmospheric physics.

Mesoscale models, in which more localized atmospheric systems forced by boundary-layer and moist processes are involved, rely strongly on the parameterization schemes by which the boundary-layer and surface processes are treated. An accurate moisture flux parameterization is crucial since surface moisture flux exerts a strong influence on the surface energy budget. So far, several types of surface moisture flux and boundary-layer parameterization schemes have been developed and widely applied in different types of models, including those of Manabe et al. (1965), Blackadar (1976, 1979), Mellor and Yamada (1974, 1982), Carlson and Boland (1978), and Zhang and Anthes (1982). Studies have tested different types of surface moisture flux schemes (Nappo 1975; Pan 1990; Argentini et al. 1992) and found that the aerodynamic formula overpredicts moisture flux from the ground. Pan (1990) showed that for a global forecast model an alternative approach based on potential evapotranspiration can alleviate this problem.

In this paper, we evaluate the performance of various alternatives to the customary aerodynamic formula for calculating the surface moisture flux in a mesoscale model [Mesoscale Analysis and Prediction System (MAPS), Bleck and Benjamin 1993; Benjamin et al. 1993]. Different parameterizations of vertical turbulent mixing above the surface are also tested.

* Permanent affiliation: Chinese Academy of Meteorological Sciences, State Meteorological Administration, Beijing, China.

** Visitor under the U.S.–Russia Bilateral Agreement on Environmental Protection.

Corresponding author address: Dr. John M. Brown, NOAA/ERL/FSL, R/E/FS1, 325 Broadway, Boulder, CO 80303.

2. Surface moisture flux and boundary-layer parameterization schemes

The surface of the earth and the atmosphere interact through fluxes of heat, moisture, and momentum at the interface. Spatial variations in these fluxes can produce significant small-scale circulations in mesoscale models so that an accurate moisture flux parameterization is important. Currently, most meso-α or regional models use the aerodynamic (bulk) formula for the surface moisture flux calculation.

a. Different types of formulations for surface exchange coefficient to include a molecular layer

The aerodynamic (AD) formula, in its simplest bulk form, parameterizes the surface moisture flux based on the moisture content difference between the ground surface and air above and the surface exchange coefficient C_q:

$$E = M\rho_a C_q V_a (q_{gs} - q_a), \tag{1}$$

where M is the soil moisture availability and $q_{gs} = q_s(T_g)$ is the saturation mixing ratio with respect to the ground surface temperature. The prediction of the ground surface temperature T_g is described in section 4a. A detailed list of symbols is given in appendix A.

Within the first few millimeters from the ground the vertical transport is accomplished by molecular diffusion rather than by turbulence (Stull 1988; Raymond and Stull 1990). Therefore, (1) should not be applied all the way down to the ground. In other words, q_v at the top of the molecular layer should be used in (1) rather than q_{gs} at the ground. Raymond and Stull (1990, hereafter referred to as RS) proposed an alternative method by matching molecular and turbulent fluxes at the top of the molecular layer (assumed to be 1 cm in depth):

$$E = M\rho_a C_q V_a C_3 (q_{gs} - q_a), \tag{2}$$

where

$$C_3 = \frac{1}{1 + (C_1/C_2)}$$

and

$$\frac{C_1}{C_2} = \frac{k^2 V_a Z_\mu}{\nu_q[\ln(Z_a/Z_0) - \psi_m][\ln(Z_a/Z_0) - \psi_h]}. \tag{3}$$

Here, C_q is computed by (7) and ν_q is the kinematic molecular diffusivity.

Within the constant stress layer, the vertical turbulent transport of moisture can be written as

$$E = \rho_a M(\nu_q + K_q)\frac{\partial q_v}{\partial z}, \tag{4}$$

where K_q is the turbulent exchange coefficient.

Integrating, assuming that the lowest model level is still within the constant stress layer,

$$q_{gs} - q_a = \frac{E}{\rho_a M}\int_0^{Z_a} \frac{1}{\nu_q + K_q}\, dz. \tag{5}$$

Carlson and Boland (1978), Anthes et al. (1987), and Zhang and Anthes (1982) added a sublayer (1 cm) to the bottom of the surface layer to account for the molecular diffusion (hereafter referred as to the two-layer aerodynamic or 2LAD scheme). They obtained an integral surface exchange coefficient for moisture

$$C_q = \frac{1}{V_a}\left(\int_0^{Z_a} \frac{1}{\nu_q + K_q}\, dz\right)^{-1} \tag{6}$$

$$= \frac{ku_*}{V_a}\left[\ln\left(\frac{ku_* Z_a}{\nu_q} + \frac{Z_a}{Z_l}\right) - \psi_h\right]^{-1}. \tag{7}$$

In this paper, we introduce yet a third approach (hereafter referred to as the three-layer aerodynamic or 3LAD scheme), a generalization of the Carlson and Boland formulation. We assume that the atmosphere between the ground surface and the first (lowest) computational level in the MAPS model ($z = Z_a$) can be represented by three layers instead of two, as in the earlier works. The bottom layer is a thin layer ($0 < z \leqslant Z_\mu$; $Z_\mu \sim 1$ mm) contiguous with the ground, in which the molecular diffusion is so dominant that $\nu_q \gg K_q$ (see Fig. 1). The second layer is a transition layer ($Z_\mu < z \leqslant Z_l$), where the magnitudes of molecular diffusion and the turbulent mixing are comparable. In this layer we assume that $K_q = ku_*(z - Z_\mu)$. The third layer ($Z_l < z \leqslant Z_a$) is the layer dominated by turbulent mixing, where $K_q = ku_*(z - Z_\mu)\phi_h^{-1} \gg \nu_q$. Here, we ignore the slight discontinuity in K_q at $z = Z_l$ and assume that $\phi_q = \phi_h$.

In this generalized aerodynamic formula, the integration in (5) is now over the three sublayers; that is,

$$C_q = \frac{1}{V_a}\left[\left(\int_0^{Z_\mu} + \int_{Z_\mu}^{Z_l} + \int_{Z_l}^{Z_a}\right)\frac{1}{\nu_q + K_q}\, dz\right]^{-1}. \tag{8}$$

Substituting the above expressions for K_q into (8), integrating segmentally, ignoring a small term involving Z_μ in the second integral, and following a procedure similar to that of Carlson and Boland (1978), we have

$$C_q = \frac{ku_*}{V_a}\left[\frac{ku_* Z_\mu}{\nu_q} + \ln\frac{ku_* Z_l + \nu_q}{\nu_q} + \ln\frac{Z_a}{Z_l} - \psi_h\right]^{-1}. \tag{9}$$

Comparing (9) and (7), one can see that the first term in the brackets on the right-hand side of (9) results from the introduction of the first layer (from 0 to Z_μ). If $Z_\mu = 0$, (9) and (7) become identical so that the three-layer formula reduces to the two-layer formula. The stability parameters ψ_m and ψ_h are expressed in

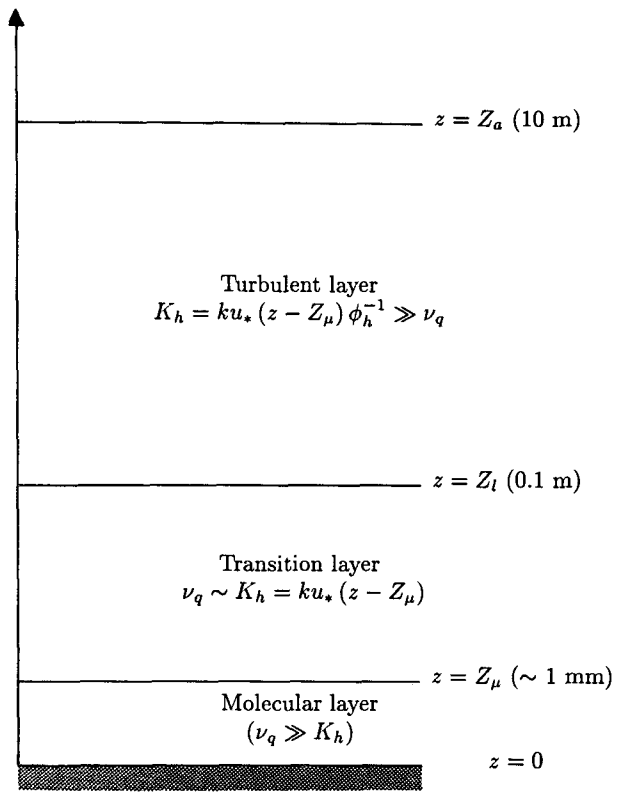

FIG. 1. Schematic diagram for 3LAD scheme showing the three-layer structure assumed for the 10-m-thick layer between the lowest MAPS computational level and the ground.

terms of the Richardson number Ri (Anthes et al. 1987; Zhang and Anthes 1982) as follows:

1) For the stable regime ($\mathrm{Ri} > \mathrm{Ri}_c$),

$$\psi_h = \psi_m = -10 \ln \frac{Z_a}{Z_0}. \tag{10}$$

2) For the mechanically driven turbulence regime ($0 \leqslant \mathrm{Ri} \leqslant \mathrm{Ri}_c$),

$$\psi_h = \psi_m = -5\left(\frac{\mathrm{Ri}}{1.1 - 5\mathrm{Ri}}\right) \ln \frac{Z_a}{Z_0}. \tag{11}$$

3) For the forced convection or quasi-neutral regime ($\mathrm{Ri} < 0$ and $|D/L| \leqslant 1.5$),

$$\psi_h = \psi_m = 0. \tag{12}$$

4) For the free convective regime ($\mathrm{Ri} < 0$ and $|D/L| > 1.5$),

$$\psi_h = -3.23\zeta - 1.99\zeta^2 - 0.474\zeta^3, \tag{13}$$

$$\psi_m = -1.86\zeta - 1.07\zeta^2 - 0.249\zeta^3, \tag{14}$$

where $\zeta = Z_a/L$.

The choice of Z_μ is quite arbitrary. An appropriate value would seem to be related to some locally defined Reynolds number, or to the proximity to the surface to which turbulent transports are important. Accordingly, we have chosen to make Z_μ inversely proportional to u_*, to wit,

$$Z_\mu \propto \frac{\nu_q}{ku_*},$$

so that the first term in the denominator of (9) is a constant. For our value of ν_q, a proportionality constant of 20.8 gives $Z_\mu = 5$ mm for a u_* value of 0.25, within the range discussed by Stull (1988) and Raymond and Stull (1990). In section 5d we discuss sensitivity experiments for various values of this constant. All other runs use the value 20.8.

b. The Penman–Monteith potential evaporation formula

Since the diurnal cycle results from solar radiation, the latent heat flux is determined not only by the vertical moisture gradient but also indirectly by radiation (via vertical mixing), at least over land where the diurnal cycle is strong. The Penman–Monteith potential evapotranspiration formula (hereafter referred to as the PM scheme, Penman 1948; Monteith 1965) computes surface moisture flux through a surface energy budget. The PM formula avoids direct use of ground surface temperature, on which the saturation mixing ratio is exponentially dependent. Our application, following Pan (1990) and Mahrt and Ek (1984), combines the aerodynamic (AD) formula with the use of the surface energy budget. Although Pan (1990) showed that the PM scheme was superior to the AD scheme in a global model, its performance in a mesoscale model has not yet been demonstrated.

The PM scheme is based on balance between all surface energy fluxes (radiative, sensible and latent heat, ground). The potential latent heat flux from the ground surface is determined as a residual using the energy budget equation. The form of the scheme (Pan 1990) used in this paper is

$$L_v E_p = \frac{(R_n - G)\Delta + (1 + \gamma)L_v E_a}{\Delta + (1 + \gamma)(1 + C_q V_a r_s)}, \tag{15}$$

where

$$L_v E_a = \rho_a L_v C_q V_a [q_s(T_a) - q_a] \tag{16}$$

$$\Delta = \frac{L_v}{c_p}\left(\frac{dq_s}{dT}\right)_{T_a}$$

$$\gamma = \frac{4\sigma T_a^3}{\rho_a c_p C_q V_a}$$

$$R_n = (1 - \beta)S\downarrow + L\downarrow - \sigma T_a^4. \tag{17}$$

The actual evaporation from the surface is obtained by multiplying the potential evapotranspiration by M.

The most serious disadvantage of the usual PM formula is the failure to include the influence of the atmospheric stability on moisture transport. Here, we follow Mahrt and Ek (1984) in adopting the following stability-dependent exchange coefficient. For $\mathrm{Ri} \leq 0$,

$$C_q = \left\{\frac{k}{\ln[(z + Z_0)/Z_0]}\right\}^2 \left[1 - \frac{15\mathrm{Ri}}{1 + C(-\mathrm{Ri})^{1/2}}\right], \tag{18}$$

where

$$C = \frac{75k^2(Z_a/Z_0)^{1/2}}{[\ln(Z_a/Z_0)]^2},$$

and for $\mathrm{Ri} > 0$,

$$C_q = \left\{\frac{k}{\ln[(z + Z_0)/Z_0]}\right\}^2 \frac{1}{(1 + 15\mathrm{Ri})(1 + 5\mathrm{Ri})^{1/2}}. \tag{19}$$

c. Comments on the moisture availability M

The term *moisture availability* was first introduced by Manabe et al. (1965) and defined as the ratio of the actual soil moisture content to its potential capacity as in (36). Since then, many researchers have used this concept as a crude empirical means of taking account of the effects of vegetation and land use in evaluation of surface moisture flux, as in (1). However, quantitative arguments justifying this common practice of multiplying by M appear to be lacking; furthermore, data allowing a determination of M through a formula like (36) are generally available only from special field projects (e.g., the O'Neill experiment, which is referred to in section 4c). The high temporal variability in rainfall and soil properties compounds these problems.

Therefore, the M values used in tests described in the following sections should be taken as relatively imprecise empirical constants except in the O'Neill case, where the observed data are available to permit us to compute M values. For the Wangara, Australia, case (also described in section 4c), soils consist largely of brown loam, 5–20 cm thick, overlying red–brown clay subsoil. It rained on day 27, one week from day 33. It was estimated that the soil was quite dry for nonrain days (Clarke et al. 1971). We also estimated the M value for the Wangara case by examining 1D predictions with various combinations of M and procedures for calculating surface fluxes. This suggested a value of $M \approx 0.25$. For the Kansas case, where only crude land-use information was available to estimate the M value, we chose different values for tests (Table 2). In all 3D experiments, M values (Table 1) are adopted from Anthes et al. (1987).

3. Parameterization of boundary-layer flux

In early atmospheric models, the boundary-layer processes were parameterized using simple, first-order closure or K theory with the vertical variation (if any) of the exchange coefficient prescribed. With progress in modeling techniques and computer power, more sophisticated schemes and higher-order closure formulations have been increasingly applied in atmospheric models. Among these, the Blackadar convective scheme and the Mellor–Yamada turbulence schemes are among the most widely used in recent years.

In both the Blackadar and Mellor–Yamada 2.0 schemes, vertical turbulence transports are diagnosed purely from mean variables without predicting the turbulence variables. Both have gained acceptance by model developers. Therefore, it is worthwhile to compare these, inasmuch as they are based on different physical grounds and yet have comparable computational requirements.

a. The Blackadar scheme

In the Blackadar convective scheme (hereafter referred to as the BL scheme, Blackadar 1976, 1979), when static instability exists near the surface, the turbulent exchange is modeled as taking place not only between two contiguous layers but throughout the whole mixed layer (Stull 1991). The model equations are briefly described as follows (see Zhang and Anthes 1982 for more details).

At model levels within the mixed layer, but above the computational level closest to the surface, for θ_v and q_v,

$$\frac{\partial \alpha_i}{\partial t} = \bar{m}(\alpha_a - \alpha_i). \tag{20}$$

For u and v,

$$\frac{\partial \alpha_i}{\partial t} = \bar{m}w(\alpha_a - \alpha_i), \tag{21}$$

$$\bar{m} = H_a\left[\rho_a c_p(1 - e)\int_{Z_a}^{D}(\theta_{va} - \theta_{vi})dz\right]^{-1}, \tag{22}$$

and

$$H_a = \rho_a c_p Z_a(\theta_{va} - \theta_{v2})^{3/2}\left(\frac{2g}{27\theta_{va}}\right)^{1/2} \times \frac{1}{Z_a}[Z_a^{-1/3} - (2Z_2)^{-1/3}]^{-3/2}, \tag{23}$$

where the subscripts a, 2, and i represent the first, second, and ith model level, respectively, and w is a weighting function that decreases linearly from 1 at the bottom to 0 at the top of the mixed layer.

Above the mixed layer, the eddy coefficient is computed as follows:

when $\mathrm{Ri} \leq \mathrm{Ri}_c$,

$$K_z = K_{z0} + l_k^2\left[\left(\frac{\partial u}{\partial z}\right)^2 + \left(\frac{\partial v}{\partial z}\right)^2\right]^{1/2}\frac{\mathrm{Ri}_c - \mathrm{Ri}}{\mathrm{Ri}_c}; \quad (24)$$

when $\mathrm{Ri} > \mathrm{Ri}_c$,

$$K_z = K_{z0}.$$

Here, K_z stands for both K_h and K_m.

b. The Mellor–Yamada scheme

Because of the computational complexity involved in higher levels of the Mellor–Yamada (MY) scheme, only the level 2.0 scheme is investigated here. This scheme assumes that the generation and dissipation of the turbulence kinetic energy (TKE) are in balance. The turbulence exchange coefficients are diagnosed purely from mean variables (Mellor and Yamada 1982). Implementation of the MY level 2.0 scheme follows Janjic (1990).

A crucial aspect of the parameterization is the definition of the master length scale. Here, we follow Eq. (50) of Mellor and Yamada (1982) and Janjic (1990) in using the expression

$$l = l_0\frac{kz}{kz + l_0}, \quad (25)$$

where

$$l_0 = \alpha\frac{\int_0^\infty |z|qdz}{\int_0^\infty qdz}. \quad (26)$$

Here, α is constant and assumed equal to 0.05. The choice of the smaller α value is based on noting that our vertical model resolution is lower than that in Mellor and Yamada (1982); this precludes capturing the detail of the vertical profile of TKE. The full set of the MY level 2.0 equations used in MAPS is given in appendix B.

4. Model and data description

a. One-dimensional model

In practice, 1D models are usually the first step to test a new scheme because they are much more economical than 3D models and they allow more carefully controlled experiments. This 1D model used here is extracted from the 3D MAPS model by assuming horizontal homogeneity. The vertical spacing is the same as that described in section 4b. The governing equations are as follows:

$$\frac{\partial u}{\partial t} = -\frac{1}{\rho}\frac{\partial\rho\overline{u'w'}}{\partial z} + f(v - V_g) \quad (27)$$

$$\frac{\partial v}{\partial t} = -\frac{1}{\rho}\frac{\partial\rho\overline{v'w'}}{\partial z} - f(u - U_g) \quad (28)$$

$$\frac{\partial\theta_v}{\partial t} = -\frac{1}{\rho}\frac{\partial\rho\overline{\theta_v'w'}}{\partial z} \quad (29)$$

$$\frac{\partial q_v}{\partial t} = -\frac{1}{\rho}\frac{\partial\rho\overline{q_v'w'}}{\partial z}, \quad (30)$$

where at the levels above the first level

$$\overline{(u, v)'w'} = -K_m\frac{\partial(u, v)}{\partial z} \quad (31)$$

$$\overline{(\theta_v, q_v)'w'} = -K_h\frac{\partial(\theta_v, q_v)}{\partial z}. \quad (32)$$

At the first model level,

$$[(\overline{u'w'})^2 + (\overline{v'w'})^2]^{1/2} = u_*^2 \quad (33)$$

$$\rho_a\overline{(c_p\theta_v, q_v)'w'} = (H, E). \quad (34)$$

All the overbars for the mean variables u, v, θ_v, q_v, and ρ are omitted. The force–restore method is used to predict the temperature at the ground surface:

$$c_g\frac{\partial T_g}{\partial t} = R_n - G - H - L_vE. \quad (35)$$

A simple cloud-interactive radiation scheme (Benjamin and Carlson 1986) is used to calculate R_n.

b. Three-dimensional model

The MAPS model is the forecast component of a four-dimensional data assimilation system that ingests observations from rawinsondes, wind profilers, commercial aircraft, and surface stations, and produces high-frequency (3-h) analyses and short-range forecasts for aviation and other mesoscale forecast users.

The recently implemented hybrid-b version of MAPS is used in this study (Bleck and Benjamin 1993; Benjamin et al. 1993). This new coordinate provides much higher vertical resolution at lower levels than the previous hybrid-a coordinate, and the transition between the θ and σ domains is continuous. The vertical model resolution in the σ domain is 2, 5, 8, 10, 15, and 20 hPa with additional 20-hPa layers until the isentropic domain is reached. In the θ domain, the isentropic resolution varies from 4 K at lower levels to 30 K at the top. Horizontal resolution is 60 km with a domain covering the contiguous United States and neighboring areas. The time step is 90 s. The model physics includes Grell's modified Arakawa–Schubert cumulus parameterization scheme (Grell 1993), a simple cloud-interactive radiation scheme (Benjamin

and Carlson 1986), Mellor–Yamada level 2.0 turbulence closure scheme, and explicit cloud physics (not activated for this study). The surface land-use characteristics used in this study are categorized into 13 types (see Fig. 2). The surface parameters of each category are listed in Table 1 (Anthes et al. 1987).

c. *One-dimensional data*

Table 2 summarizes all datasets for this study. For 1D simulations, three cases are selected representing different meteorological conditions. The first one, a dry winter case, is the Wangara, Australia, day 33 (Clarke et al. 1971), which has been used extensively to test planetary boundary layer (PBL) models. To conform with other studies on this dataset, the integration started at 0900 LST and continued until 1800 LST (see Table 2).

The second case, a hot, moist summer case, is within the domain of the MAPS assimilation system. To be representative of initial conditions for the 3D MAPS forecast model, instead of initializing the model with a real sounding at a station, we chose analyzed conditions at a model grid point. The central grid point of the MAPS domain (39.6°N, 98.6°W, 550 m above sea level), located in northern Kansas, was selected (hereafter referred to as the "Kansas case"). Initial conditions for the 1D integration were at 0600 UTC 24 August 1991. The 0600 UTC starting time, corresponding to 0000 LST, is chosen to include the complete diurnal cycle. The wind, temperature, and moisture profiles at this grid point were directly fed into the 1D model without further vertical interpolation. The 1D experiments for this case were run in the hybrid-a coordinate (30-hPa resolution through approximate 150 hPa AGL, isentropic above) since the original data were not available for the hybrid-b coordinate.

Weather conditions for the Kansas case were rather typical for late summer. Moderately humid near-surface air was surmounted by a strong cap of elevated mixed-layer air that had been heated over the western United States. A moderate southerly low-level jet at less than 10 m s^{-1} existed. Between 700 and 400 hPa,

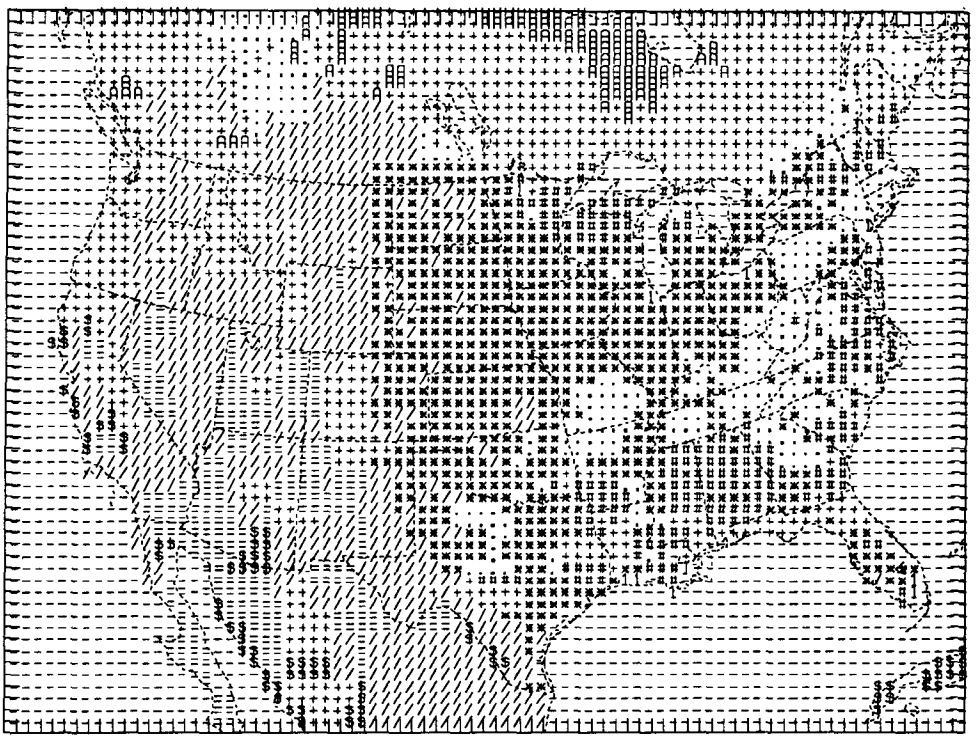

FIG. 2. Distribution of land-use types in the MAPS model domain.

TABLE 1. Various surface parameters for different land-use types (for summer) in the MAPS model domain.

Category	β (%)	M (%)	ϵ (%)	Z_0 (cm)
Urban land	18	5	88	50
Agriculture	17	30	92	15
Range grassland	19	15	92	12
Deciduous forest	16	30	93	50
Coniferous forest	12	30	95	50
Mixed forest and wetland	14	35	95	40
Water	8	100	98	0.0001
Marsh or wetland	14	50	95	20
Desert	25	2	85	10
Tundra	15	50	92	10
Permanent ice	55	95	95	5
Tropical or subtropical forest	12	50	95	50
Savannah	20	15	92	15

light easterly or northeasterly winds were less than 5 m s^{-1}. Above that, winds were northerly at 10–15 m s^{-1}. The sounding shows that the analysis contained a temperature inversion between the lowest two analysis levels, with a suggestion of a "residual layer" of lower static stability above, left over from the previous day's mixed layer. Overall, low-level temperature and moisture advection was weak.

One can see later that the results obtained from the Wangara and Kansas cases are somewhat dependent on M. Since no specific information was available for deducing M for the above two cases, we choose the O'Neill experiment as the third case.

The O'Neill field experiment was part of the Great Plains Turbulence Field Program. The experiment site was fairly flat rangeland and located about 5 miles east-northeast of the town of O'Neill, Nebraska. The O'Neill exploration was a very comprehensive field experiment that produced many soil moisture and temperature measurements. The dataset from the O'Neill experiment (Lettau and Davidson 1957) contained several general observation periods; each lasted about 24 h. We chose the third one extending from 1835 LST 18 August to 1835 LST 19 August 1953; this period appeared to be dominated by diurnal changes.

TABLE 2. Description of the data for this study.

Dimension	Description	Duration	M
1D	Wangara day 33	0900–1800 LST	0.25
	Kansas 24 August 1991	0000–2400 LST	0.05–0.5
	O'Neill third period	1835–1835 LST	Diagnostic
3D	8 March 1992	1200–0000 UTC	Climatological
	12 August 1992	1200–0000 UTC	Climatological
	13–28 May 1993	1200–0000 UTC	Climatological

TABLE 3. Description of main experiments.

Experiment	Description	Moisture flux scheme	PBL scheme
1.1	Flux matching (1D)	RS	MY
1.2	Two layer (1D)	2LAD	MY
1.3	Three layer (1D)	3LAD	MY
1.3A	Blackadar (1D)	3LAD	BL
1.4	Penman–Monteith (1D)	PM	MY
1.5	Sensitivity to Z_u (1D)	3LAD	MY
3.2	Two layer (3D)	2LAD	MY
3.3	Three layer (3D)	3LAD	MY
3.3A	Blackadar (3D)	3LAD	BL
3.4	Penman–Monteith (3D)	PM	MY

For the O'Neill case only, we diagnosed the temporal variation of M from observed soil moisture content; namely,

$$M = \frac{W_g}{W_{\max}}, \tag{36}$$

where W_g is volumetric moisture content of soil predicted using Deardorff's force–restore formula (Deardorff 1978).

d. *Three-dimensional data*

One purpose of the 3D simulations is to test the performance of schemes in horizontally variable conditions. For 3D simulations, most of the tests were run in real time for the 16-day period of 13–28 May 1993. This period is divided into two segments: 13–22 May for testing different surface moisture flux schemes, and 23–28 May for testing the PBL parameterization schemes. (The PBL experiment was stopped after 6 days because the trend was consistently clear.)

The synoptic situation over the United States was typical for the season. Medium and short waves consistently passed through this area producing much convective rainfall, especially in the central and southern United States.

To represent conditions in other seasons, we also conducted tests for winter and summer cases: 1200 UTC 8 March 1992 and 1200 UTC 12 August 1992. The first case included the beginning of the 8–9 March 1992 blizzard, one of heaviest snowfalls in the past several years in Boulder, Colorado. A maximum of about 75 cm of snowfall was observed. The second one was a typical summer day over all of the United States. Both of these experiments were run in the hybrid-a coordinate since the original data were not available in the hybrid-b coordinate.

e. *Experiment design*

The experiments are listed in Table 3. Each of the 1D experiments consists of individual runs on the

Wangara, Kansas, and O'Neill case days. Experiments 1.1, 1.2, 1.3, and 1.4 are designed to test different surface moisture flux schemes in 1D. Four moisture flux schemes are tested: RS, 2LAD, 3LAD, and PM. The MY scheme is used as the PBL scheme while testing the moisture flux schemes for both 1D and 3D experiments. Experiment 1.3A is intended to test the Blackadar (BL) scheme by comparing it with experiment 1.3. In experiment 1.3A, the 3LAD scheme is used to compute surface moisture flux for the Wangara and O'Neill cases, and PM for the Kansas case. (This latter run was performed in the hybrid-a coordinate.) Experiment 1.5 is used to test the sensitivity of results to molecular layer thickness Z_μ. The value of the dimensionless constant ku_*Z_μ/ν_q is set to 20.8 for other experiments. Experiments 3.2, 3.3, 3.3A, and 3.4 are the 3D counterparts of 1D experiments 1.2, 1.3, 1.3A, and 1.4. Because of computational limitations on the number of real-time parallel tests, no 3D experiments were performed using the RS scheme.

One-dimensional experiments are integrated for 24 h for the Kansas and O'Neill cases and 9 h for the Wangara case. The integrations are started at different hours of the day depending on data availability and comparability with other studies. Due to computing constraints and the limitation that MAPS is configured to make only short-range forecasts, all 3D experiments are integrated for 12 h starting at 1200 UTC, covering the daytime heating period. To isolate the effects of surface moisture flux, the sensible heat and momentum fluxes are all computed as described in Anthes et al. (1987).

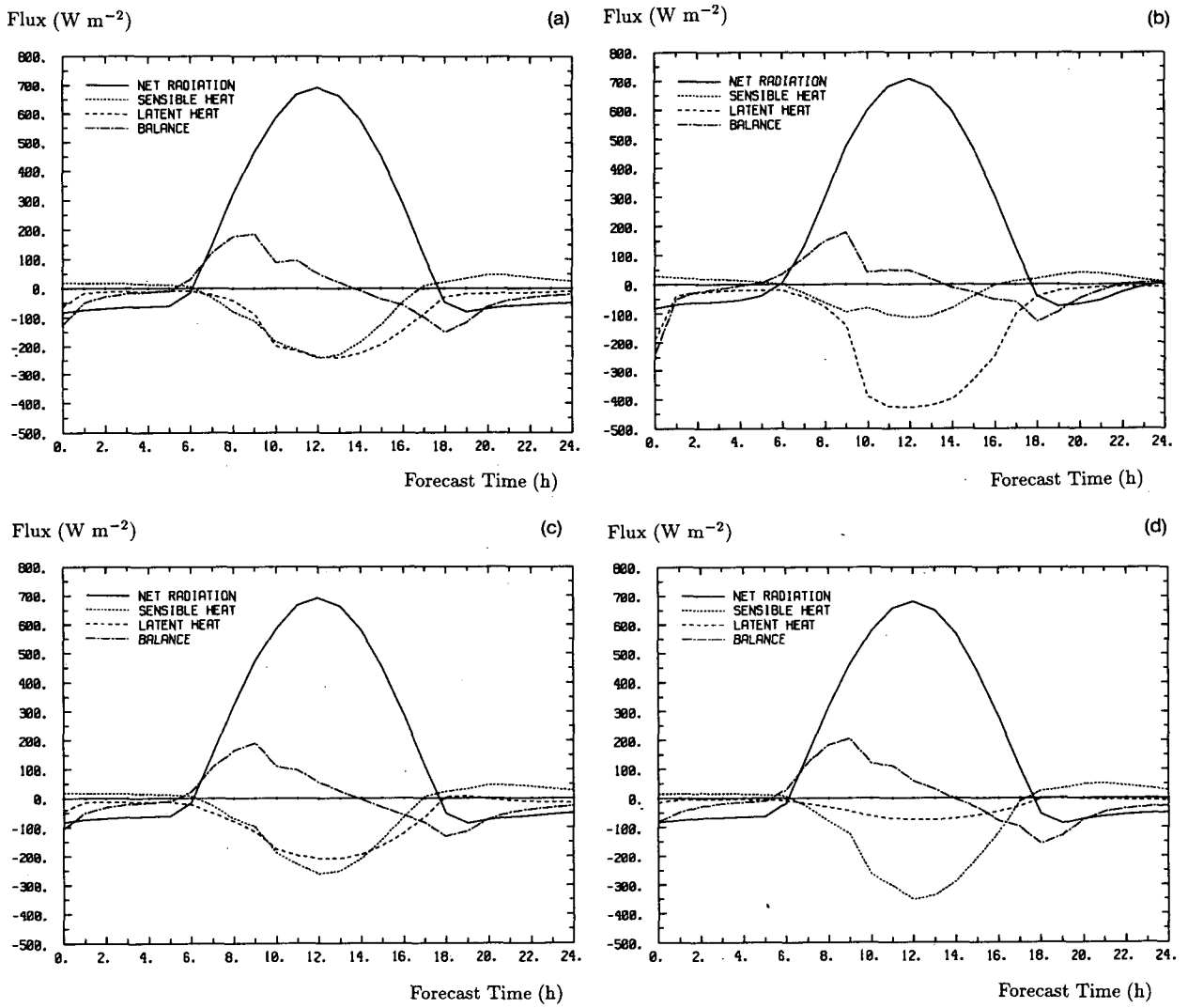

FIG. 3. Diurnal cycle of different components of the surface energy balance equation: (a) 2LAD with $M = 0.1$, (b) 2LAD with $M = 0.3$, (c) PM with $M = 0.1$, and (d) PM with $M = 0.3$.

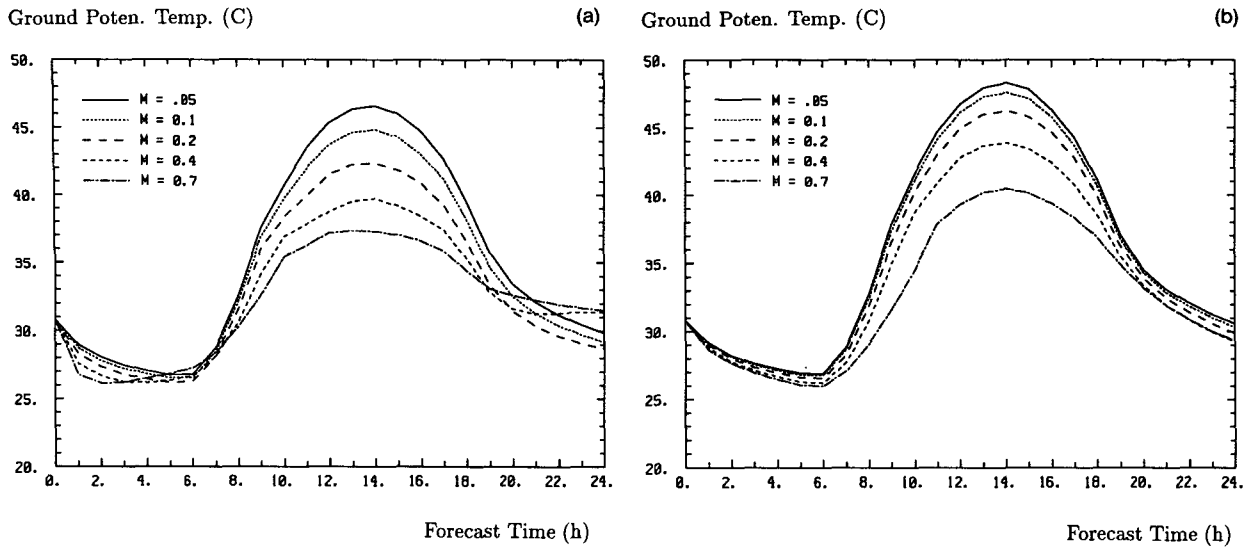

FIG. 4. Diurnal variation of ground surface potential temperature (°C) predicted by (a) 2LAD and (b) PM schemes for Kansas case.

5. One-dimensional simulation results

a. Surface comparison among different moisture flux schemes

Figure 3 shows the flux components computed for the Kansas case by the 2LAD and PM schemes. Because no clouds form in this 1D simulation, the net radiation is basically the same for the four integrations with a maximum of about 700 W m^{-2} at local noon. The heat fluxes into the ground also do not differ significantly between the two schemes (not shown). The greatest difference between the two methods is in the sensible and latent heat fluxes. For the 2LAD method, when $M = 0.1$ (Fig. 3a), the sensible heat flux is a little larger in the morning and somewhat smaller in the afternoon than the latent heat flux. When $M = 0.3$ (Fig. 3b), the latent heat flux is several times larger than the sensible heat flux. For the PM method, with $M = 0.1$ (Fig. 3c), sensible heat flux is about five times larger than the latent heat flux, whereas with $M = 0.3$ (Fig. 3d), the relationship between sensible and latent heat fluxes is similar to that when $M = 0.1$ with the 2LAD procedure.

We further varied M values from 0.05 to 0.4 to see the response in Bowen ratio B, the ratio of the sensible to latent heat fluxes ignoring their signs, to the M change. For this range of M, B varies between 2.2 and 0.1 for the 2LAD and between 10.0 and 0.4 for PM schemes, respectively. All B values in the 2LAD scheme are below 1.0 when $M \geq 0.1$. Roughly, B predicted by the PM scheme is four times larger than that computed by the 2LAD scheme.

Figure 4 shows the diurnal cycle of the ground surface potential temperature simulated by the 2LAD and PM schemes for different M values. For both methods, the surface temperature decreases with increasing M because a larger fraction of heat energy escapes from the ground as latent heat flux. For small M (0.05–0.2), comparison between Figs. 5a and 5b shows the greater sensitivity of afternoon ground temperature to the choice of M when the 2LAD scheme is used. For example, the amount of temperature increase that results from the change in M from 0.1 to 0.05 is close to the amount that results from the change in M from 0.7 to 0.4. On the other hand, the PM scheme exhibits an approximately linear relationship between M and ground temperature.

The general character of the diurnal variation of ground temperature is similar between the two schemes. It can also be seen from Fig. 3 that the balance or residual among different components in the surface energy budget equation is comparable, although huge differences exist in the sensible and latent heat fluxes themselves. Since the net radiation is essentially the same and heat flux into the ground does not differ substantially, the main difference between these two methods is the partitioning between the sensible and latent heat fluxes for a given M. This difference affects not only the ground temperature but also the thermodynamic characteristics of the mixed layer (Segal et al. 1992).

Figure 5 shows sensible and latent heat fluxes predicted by the RS, 2LAD, 3LAD, and PM schemes for the Wangara case. The 2LAD gives the smallest peak sensible heat flux of about 220 W m^{-2} (Fig. 5a) and the 3LAD gives the largest, 255 W m^{-2}. The peak sensible heat fluxes given by the PM and RS schemes are about 235 W m^{-2}. The latent heat flux simulated by

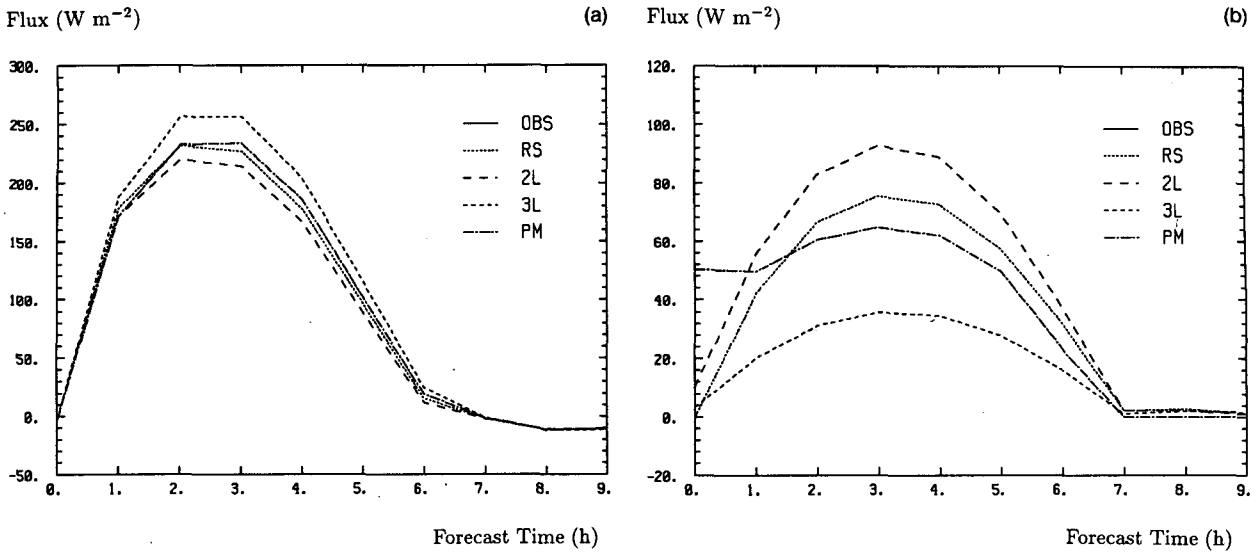

FIG. 5. Temporal variation of surface heat fluxes predicted using different surface moisture flux schemes for Wangara day 33. Hour 0 is at 0900 LST: (a) sensible heat flux and (b) latent heat flux.

the 3LAD scheme is considerably smaller than the other three schemes (Fig. 5b). The 2LAD scheme gives largest latent heat flux, and the RS and PM are the second and third, respectively.

No directly observed sensible and latent heat fluxes are available for the Wangara case. However, they can be estimated from other observations. The sensible heat flux can be deduced from temperature gradients at 1 and 2 m (Yamada and Mellor 1975). The net radiation and heat flux into the ground were observed in the Wangara dataset (Clarke et al. 1971). The latent heat flux then can be computed from energy budget equation.

The sensible heat fluxes predicted by the four schemes are generally larger than the deduced values, of which the maximum is about 210 W m^{-2}. The 3LAD scheme gives the largest sensible heat flux due to its smallest latent heat flux. The latent heat flux deduced is quite small, about 20–30 W m^{-2} around noon. This is reasonable, since the surface condition was quite dry. Thus, the latent heat flux simulated by the 3LAD is much closer to the values deduced than the other

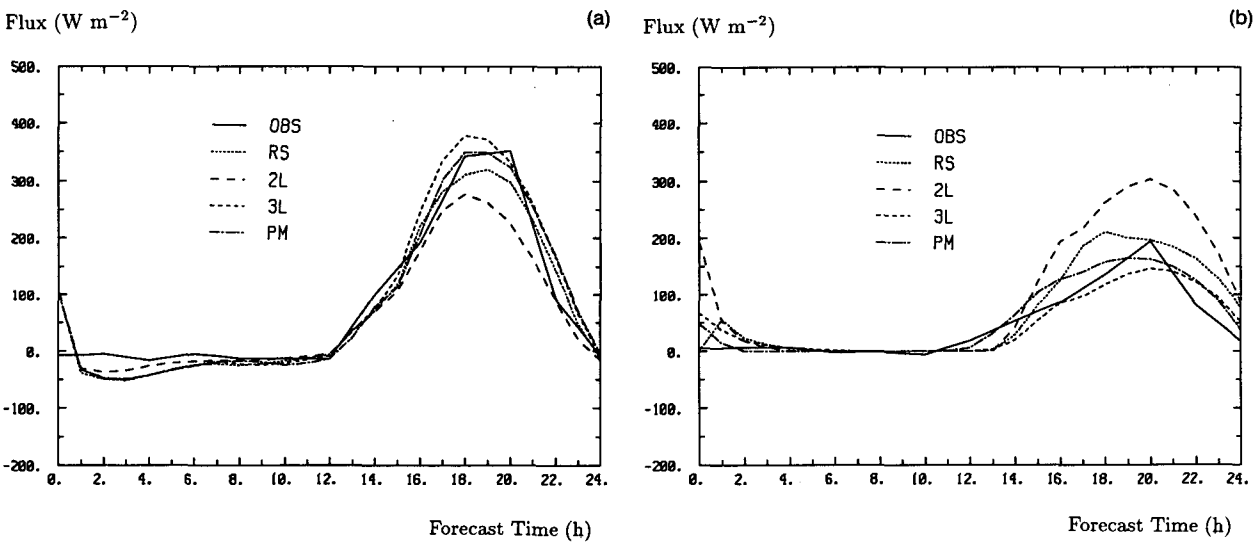

FIG. 6. As Fig. 5, for the O'Neill case. Hour 0 is at 1835 LST.

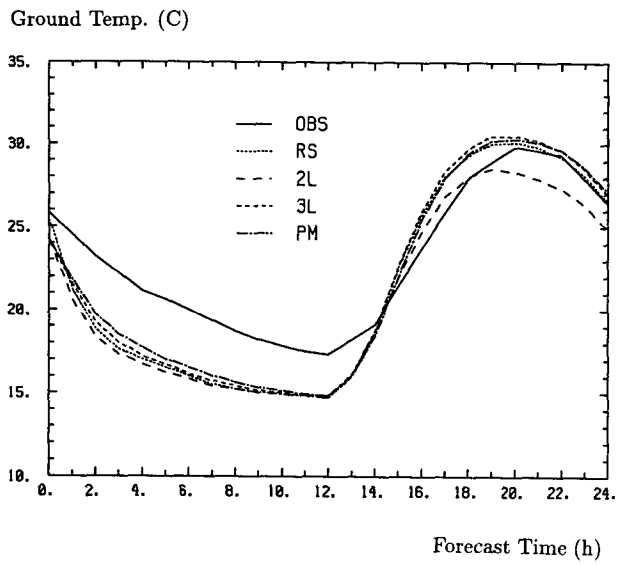

FIG. 7. As Fig. 6, for diurnal variation of ground surface temperature (°C).

three schemes. The 2LAD scheme gives a latent heat flux value that is two to three times larger than the deduced value. The PM and RS scheme computed values are too large, also.

Figure 6 shows sensible and latent heat flux for the O'Neill case. The figure also shows fluxes listed in Lettau and Davidson (1957) that are directly deduced from the observations.[1] Overall, the sensible heat flux is well simulated, especially in the early morning and late afternoon. Again, the 3LAD scheme gives the largest sensible heat flux and the 2LAD scheme gives the smallest. The 2LAD scheme yields values of sensible heat flux that are too small, about 100 W m^{-2} lower than the observed value in the late afternoon. The PM scheme's flux is closest to the observed value and somewhat better than the 3LAD and RS schemes. Figure 6b shows the latent heat flux. Almost all the schemes overpredict the latent heat fluxes. The 2LAD value is about double the observed value. The 3LAD scheme gives the most accurate flux value. If we examine total latent heat flux over the whole period of the integration, the 3LAD's total latent heat flux is close to the observed one.

Figure 7 shows computed ground surface temperature for the O'Neill runs of experiments 1.1–1.4 of Ta-

[1] Lettau and Davidson (1957) list three sets of flux values deduced using three different theoretical models. We choose the values given by Lettau's model since they behave more smoothly.

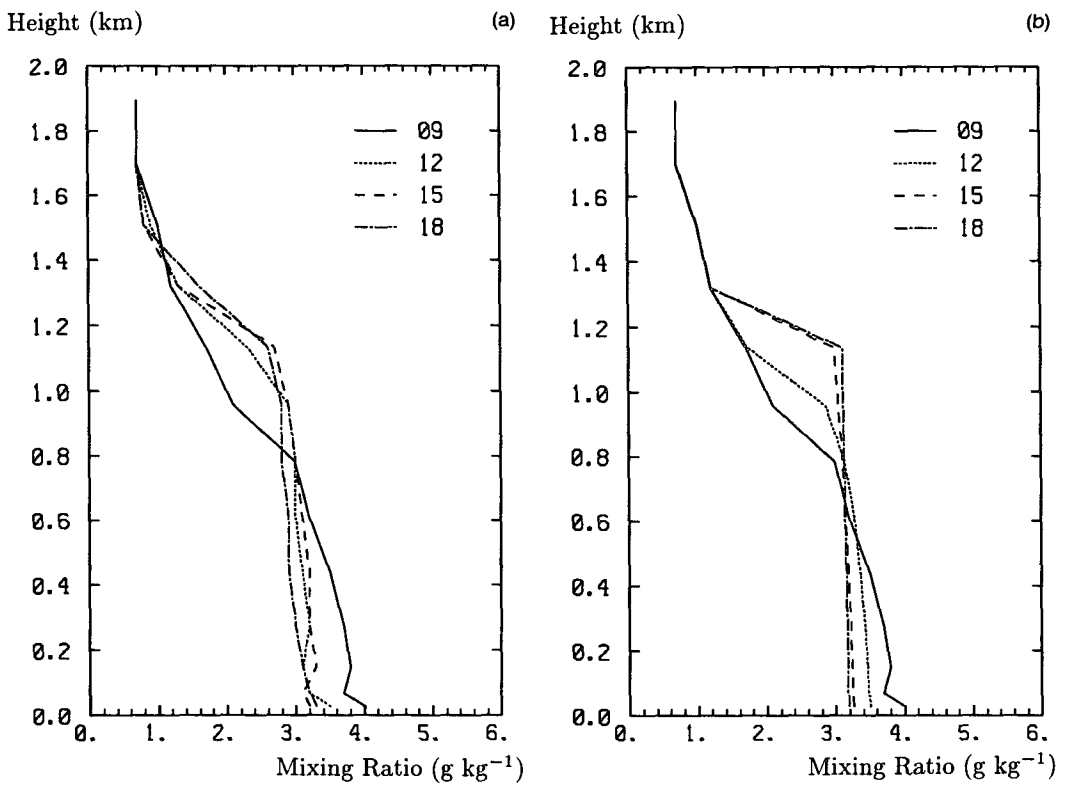

FIG. 8. Temporal variation of the mixing ratio profiles for Wangara day 33: (a) observed (hour labels in local time) and (b) forecast profiles predicted using the MY scheme for PBL parameterization and 3LAD for surface moisture flux scheme.

ble 3. The 2LAD scheme predicts a lower temperature than the other three schemes. This is due to the larger latent heat flux (Figs. 6a,b) into the atmosphere, which makes the total heat flux into the atmosphere slightly larger in 2LAD than with the other three schemes. During the afternoon, it gives a temperature about 2 K lower than do the other three schemes. Compared to the observed soil temperature at the 4.5-cm depth, which roughly corresponds to the average temperature in the top 10 cm of soil, temperature is much better simulated during the daytime than during the night. The warm bias is about 2 K in the day, while the cold bias during night is around 4 K, possibly resulting from the use of too low a reservoir temperature. The predicted temperature also has about an hour phase advance over the measured.

In summary, for warm season cases (Kansas and O'Neill), the 2LAD scheme gives latent heat flux that is too large and sensible heat flux that is too small. The 3LAD produces more reasonable values of both sensible and latent heat flux. For the cold season case (Wangara), the 3LAD scheme may slightly overpredict the sensible heat flux, but for the latent heat flux, it is more accurate than the other schemes.

b. *Profile comparison among different moisture flux schemes*

In this section, the performance of different formulations for surface moisture flux in conjunction with the MY 2.0 parameterization of vertical mixing will be compared and examined against observed profiles for the three cases. We first compare the predicted and observed moisture profile variation in time to see how the performance of the model is in general. Figure 8a shows the observed time variation of mixing ratio profiles for the Wangara case. At 0900 LST, when the integration starts, the surface mixing ratio is about 4.0 g kg^{-1}. It decreases upward gradually to 3.0 g kg^{-1} at 600 m. Above 700 m, it decreases more rapidly with height to 0.7 g kg^{-1} at 1700 m. As the mixed layer deepens, the predicted mixing ratio becomes nearly uniform within it, resulting in slight drying near the surface but considerable moistening above 700 m. Overall, the predicted vertical and temporal distributions using the 3LAD and MY schemes (Fig. 8b) are very similar to the observed ones (Fig. 8a).

Figure 9 shows the predicted and observed mixing ratio profiles for the three cases. All the schemes capture the well-developed daytime mixed layer, especially in the Wangara case. However, mixing ratio is consistently overpredicted. The difference among various schemes is mainly in the magnitudes of mixing ratio in the well-mixed layer.

Figures 9 and 10 depict the predicted and observed mixing ratio and virtual potential temperature profiles for the three cases. All the schemes capture the development of a mixed layer, particularly in the Wangara case where it was particularly well developed and well documented. For this case, mixing ratios are consistently overpredicted and temperature is underpredicted. Again, the best predictions result from the 3LAD procedure, with the 2LAD performing most poorly, although the depth of the mixed layer is predicted well by all the schemes.

For the two summer cases, both temperature and mixing ratio are consistently overpredicted. Consistent with error patterns we have noted earlier, however, the overprediction of mixing ratio is most severe with 2LAD, and least with 3LAD, with the converse being true for predictions of virtual potential temperature. We speculate that synoptic processes are responsible for the overpredictions in the O'Neill case.

c. *Comparison of the Blackadar and Mellor–Yamada schemes*

In this section we present the comparisons between the BL and the MY parameterizations of vertical turbulent mixing. Figures 11 and 12 depict this comparison. The MY scheme systematically produces a more thoroughly well mixed layer, particularly in mixing ratio, than does the BL scheme. The BL parameterization tends to excessively dilute the top portion of the mixed layer with dry air (e.g., Fig. 11a) but tends to keep the lower and middle portions of the mixed layer too moist (Figs. 11a–c). The MY procedure, on the other hand, more often than not produces a mixed layer with a more uniform mixing ratio distribution than observed (see also Figs. 8b and 9). Virtual potential temperature profiles (Fig. 12), including the implied mixed-layer depth, are more similar between the two schemes. This is probably because the (virtual potential) temperature gradient near PBL top is much smaller than that of the mixing ratio.

One may note, by comparing Figs. 11a and 12a, that the BL scheme gives a lower temperature of 2 K but larger mixing ratio of 0.8 g kg^{-1} than the MY scheme for the Wangara case. This occurs in spite of slightly larger sensible heat flux when the BL scheme is used. The explanation lies in a larger downward turbulent heat flux at the top of the mixed layer produced by the MY scheme. This downward mixing is also responsible for the overall drier mixed layer. The same situation is true for the O'Neill case and, to a much smaller extent, for the Kansas case where the stability above the top of the PBL is much weaker.

We also examined the temporal variations of mean turbulent coefficient K_h averaged over the whole boundary layer for the Kansas case. For the BL scheme, we approximate K_h under the free convective regime by the formula $\bar{m}\Delta z^2$. The BL scheme produces discontinuities in the temporal variation in implied K_h;

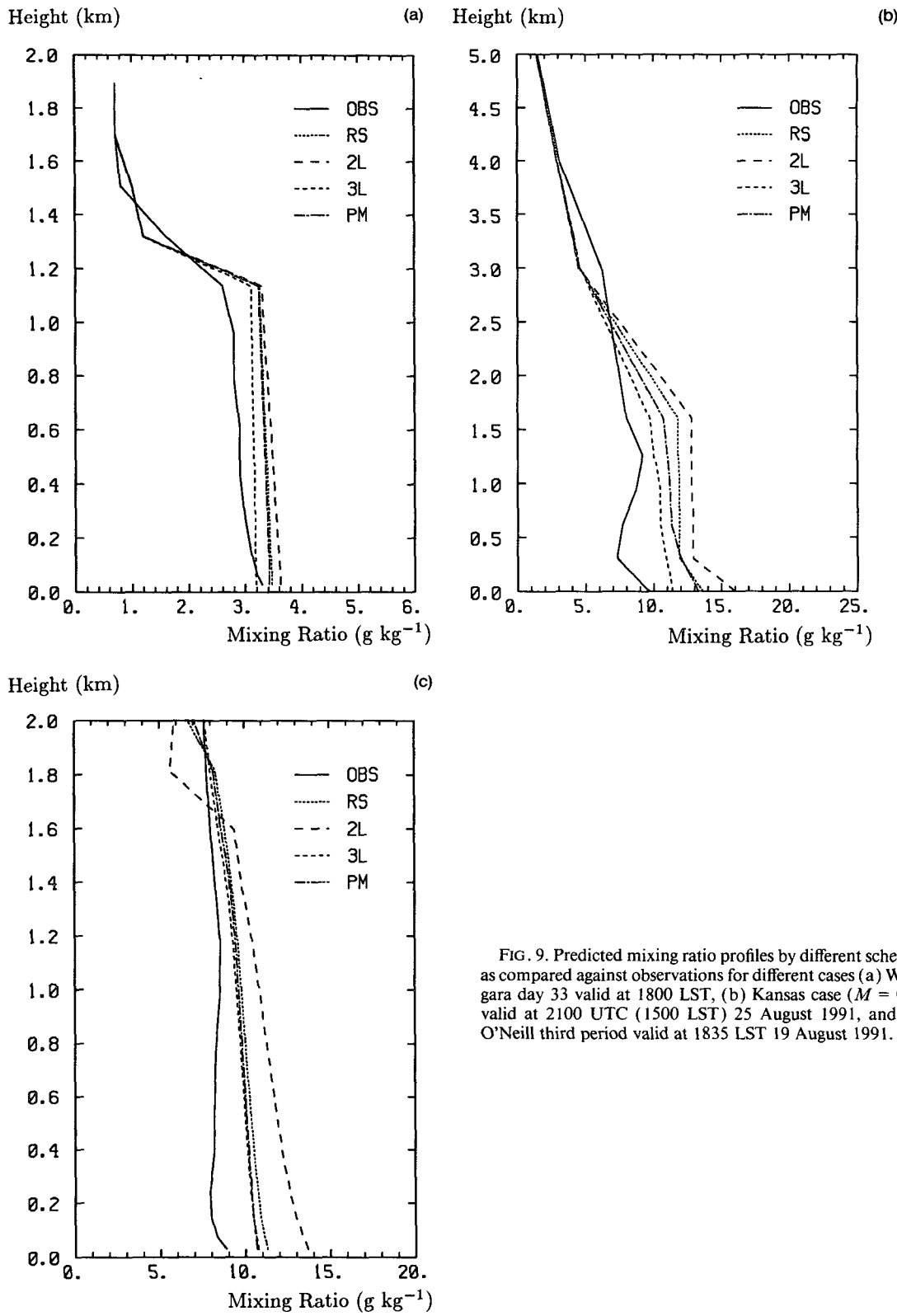

FIG. 9. Predicted mixing ratio profiles by different schemes as compared against observations for different cases (a) Wangara day 33 valid at 1800 LST, (b) Kansas case (M = 0.2) valid at 2100 UTC (1500 LST) 25 August 1991, and (c) O'Neill third period valid at 1835 LST 19 August 1991.

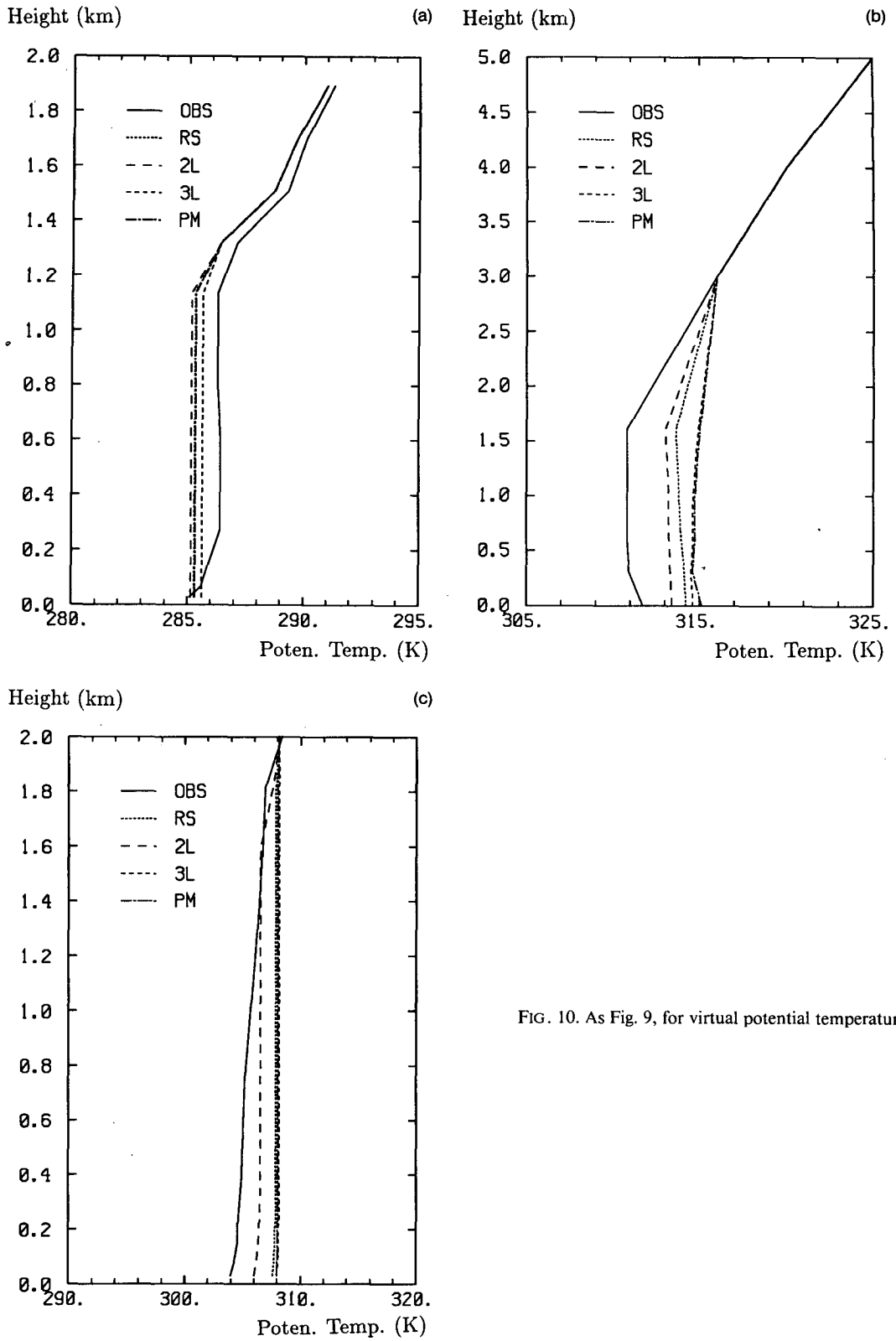

FIG. 10. As Fig. 9, for virtual potential temperature.

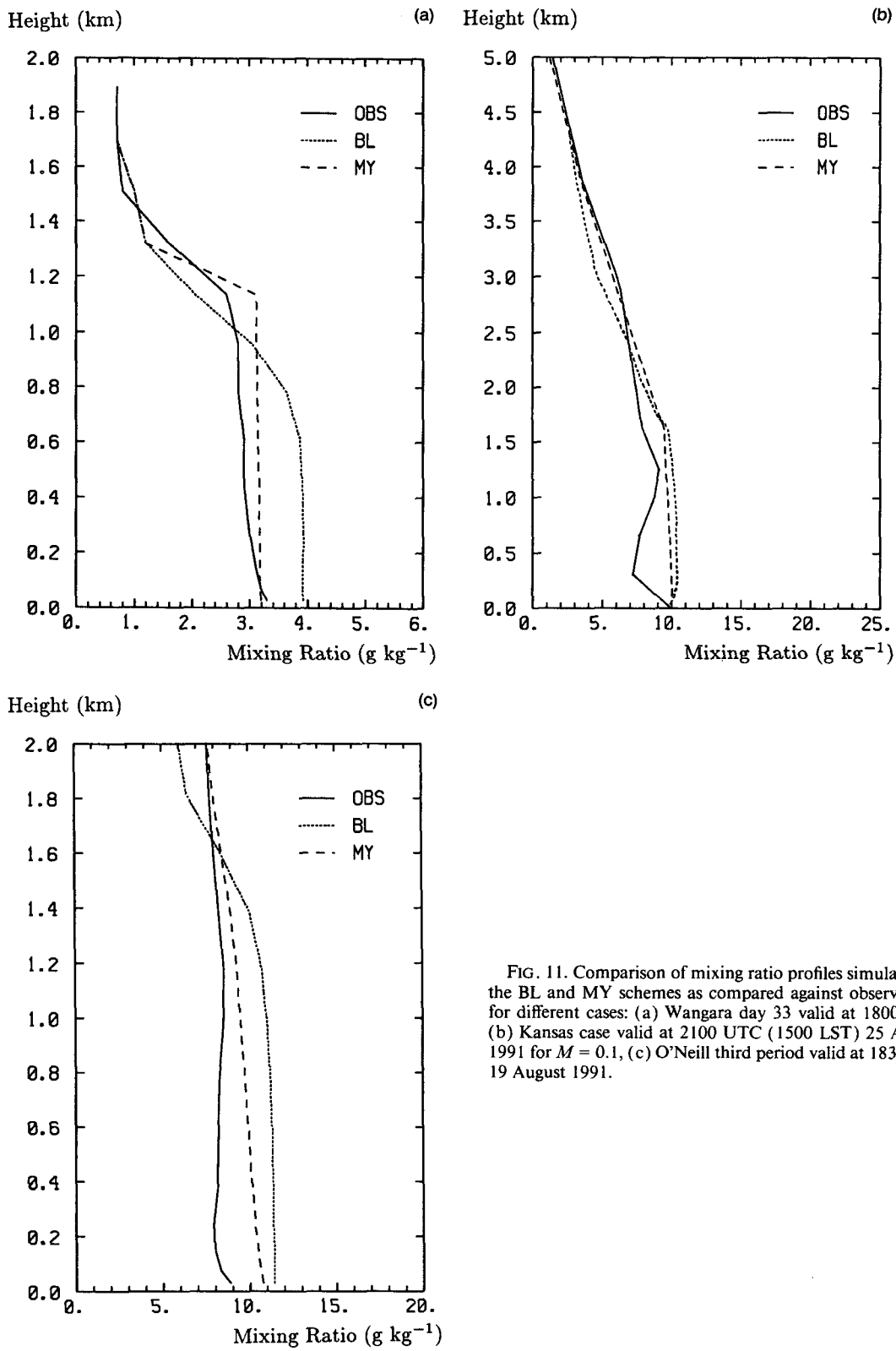

FIG. 11. Comparison of mixing ratio profiles simulated by the BL and MY schemes as compared against observations for different cases: (a) Wangara day 33 valid at 1800 LST, (b) Kansas case valid at 2100 UTC (1500 LST) 25 August 1991 for $M = 0.1$, (c) O'Neill third period valid at 1835 LST 19 August 1991.

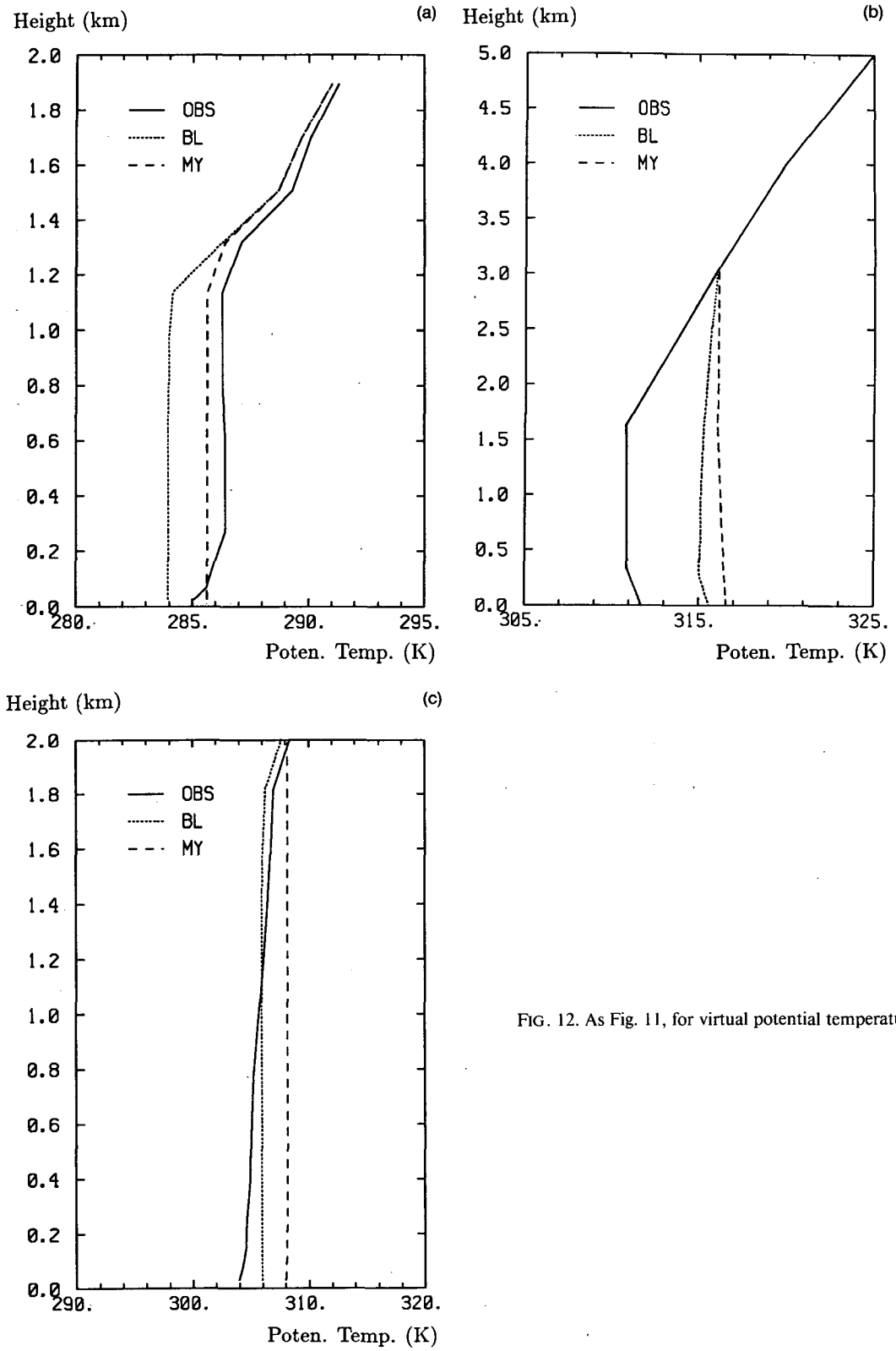

FIG. 12. As Fig. 11, for virtual potential temperature.

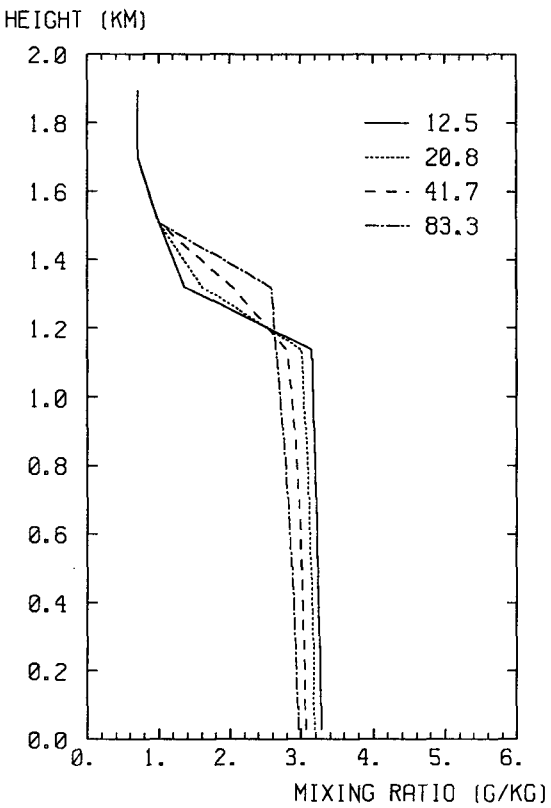

FIG. 13. Predicted mixing ratio profiles by the 3LAD scheme with the indicated values of ku_*Z_μ/ν_q for Wangara case. Legend shows Z_μ in millimeters.

the maximum value of implied K_h is about 10 m^2 s^{-1}. The MY scheme gives a smoother variation in K_h though its value is about 10 times larger than that with the BL scheme, consistent with its characteristically more uniform mixing ratio in the mixed layer. It is found that the discontinuity in the BL scheme results from the transitions among different stability regimes, especially the transition from forced to free convection, or vice versa.

For comparison, we also test a different value of α in (26). When α = 0.1 (not 0.05), as suggested by Mellor and Yamada (1982), the magnitude of K_h increases about by four times because K_h is proportional to l^2 except near the surface.

d. *Sensitivity to molecular layer thickness Z_μ*

Figure 13 shows the influence of Z_μ on mixing ratio profiles for the Wangara case. These results are presented in terms of values of the constant ku_*Z_μ/ν_q. (For reference, these values correspond to Z_μ of 1.5, 3, 5, and 10 mm, respectively, for u_* = 0.5 m s^{-1}.) Mixing ratio differences between these runs are in the sense expected from inspection of (9); a deeper molecular layer concentrates more of the vertical gradient in mixing ratio very close to the surface, thus reducing the value of the exchange coefficient and the surface moisture flux.

We also compared the sensitivity of moisture profiles to Z_μ between the RS and 3LAD schemes. For the same range of the Z_μ value, the mixing ratio changes by about 20%–60% more in the RS than with the 3LAD scheme through most of the mixed layer (not shown). Thus, the sensitivity to Z_μ is weaker in the 3LAD than in the RS scheme. In fact, this can be seen from (3) and (9). In (3), C_3 and, in turn, the moisture flux, are almost inversely proportional to Z_μ since the value of C_1/C_2 is larger than 1. On the other hand, in (9) the Z_μ term is comparable to the other terms. Thus, the sensitivity to Z_μ is weaker in the 3LAD than in the RS scheme.

6. Three-dimensional simulation results

a. *Comparison among different moisture flux schemes*

In this section, we will examine results from 3D experiments testing the surface moisture flux schemes. Figures and tables presented in this section are for results averaged over a 10-day period of parallel runs with the MAPS model using different schemes. Figure 14 shows the mean 12-h forecast errors (forecast minus analyzed) over the 10-day period in relative humidity RH at the surface (10 m AGL) produced using the 2LAD, PM, and 3LAD schemes. Since the verifying analyses use a background from a forecast using the 3LAD scheme and since there are observations that correct that forecast generally only over land, we will ignore differences over oceanic areas.

All three formulas give mostly positive errors (too moist forecasts). However, the error distributions and magnitudes are quite different. For the 2LAD scheme (Fig. 14a), the largest errors over land are over the southwestern United States, especially in high-terrain regions, over the southeastern United States, and over the Great Lakes region. Mean errors in these regions are over 32% and reach near 40%. The errors in high-elevation regions for the 2LAD scheme are likely related to high surface temperatures and perhaps also to improper specification of M for this particular time period. These errors are reduced somewhat using the PM scheme (Fig. 14b) and further still with the 3LAD scheme (Fig. 14c). The maximum errors using the 3LAD scheme are reduced in these same regions to 20%–25%. The minimum mean error over land with all three schemes is over the Great Plains (from Oklahoma to Nebraska). This area with a slight negative error (too dry forecast) using both the PM and 3LAD schemes received above-normal precipitation during this period, implying that the climatological specification of M was probably too low. Overall, the 3LAD

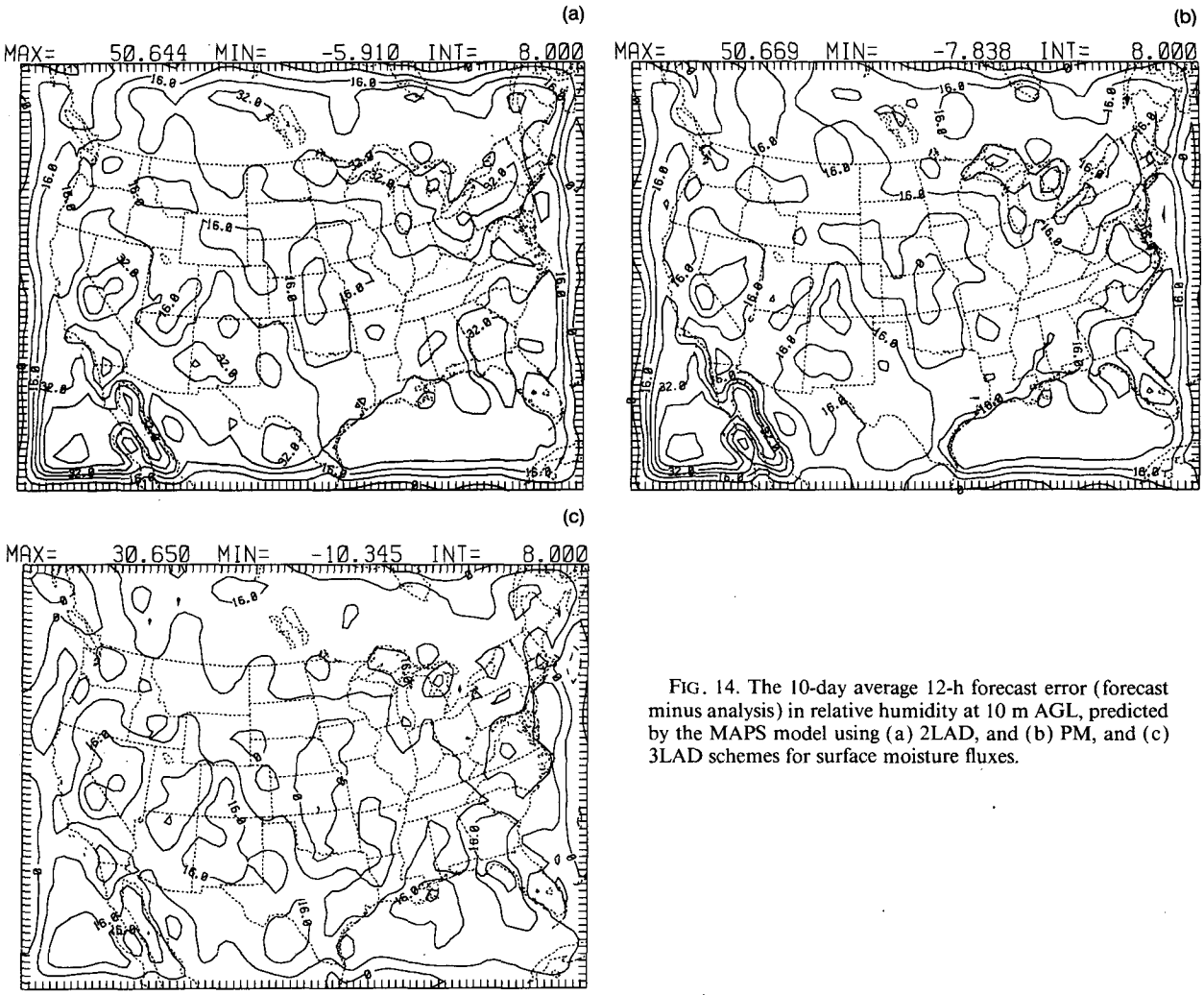

FIG. 14. The 10-day average 12-h forecast error (forecast minus analysis) in relative humidity at 10 m AGL, predicted by the MAPS model using (a) 2LAD, and (b) PM, and (c) 3LAD schemes for surface moisture fluxes.

scheme mean errors are lower than for either of the other schemes.

The relative humidity errors at the fifth model level (25 hPa AGL, no figures shown) are positive over most of the domain but the magnitudes are much smaller than those at the surface. At the same time, the negative errors are slightly increased in magnitude compared to those at the surface. The errors at this level are more uniformly distributed over the whole domain. Among the three schemes, the 3LAD scheme again best predicts relative humidity, and the 2LAD scheme produces the largest errors.

Table 4a lists the 12-h forecast rms errors over the whole domain in relative humidity and temperature using the 2LAD, PM, and 3LAD schemes at the surface and the fifth level. These are dominated by differences over land where results are considered to be meaningful, but there is a smaller influence from results over oceanic areas that are not considered to be reliable. At the surface level, the 3LAD gives smallest rms error at 15.6%, the PM scheme gives the second smallest at 21.5%, and the 2LAD scheme gives the third smallest at 26.0%. At the fifth level (Table 4a), the 3LAD, PM, and 2LAD rms errors are 15.2%, 17.5%, and 20.8%, respectively.

For the 9 March 1992 blizzard (winter) and 1200 UTC 12 August 1992 (summer) cases (no figures or tables shown) the 3LAD gives better moisture forecasts than the 2LAD and is comparable or slightly better than the PM scheme. The improvement is more evident near the ground than at the higher levels and more in summer than in winter, which should be the case since surface moisture fluxes are large in summer. Thus, the results from the individual summer and winter cases are consistent with the 10-day average in May.

Relative humidity depends not only on mixing ratio but also on temperature. In contrast to the relative humidity errors, the rms temperature errors show little variation among the different moisture flux schemes. The PM scheme is very slightly better than the other two schemes. Thus, differences in relative humidity

TABLE 4. (a) Ten-day-averaged rms errors (defined as difference between forecast and verifying analysis) in relative humidity and temperature by the three-layer (3LAD) and two-layer aerodynamic (2LAD) formula and Penman–Monteith (PM) schemes at two model levels. (b) Six-day averaged rms errors in relative humidity and temperature by the Blackadar (BL) and Mellor–Yamada (MY) schemes.

Variable	Level	3LAD	PM	2LAD
(a)				
Relative humidity (%)	1	15.6	21.5	26.0
	5	15.2	17.5	20.8
Temperature (K)	1	4.2	4.1	4.4
	5	4.0	3.8	4.0
		BL	MY	
(b)				
Relative humidity (%)	1	40.7	25.7	
	3	35.9	23.9	
	5	23.0	19.2	
Temperature (K)	1	7.1	4.4	
	3	5.3	4.0	
	5	4.2	3.6	

errors among different schemes are mostly a result of differences in mixing ratio rather than temperature.

Regarding the use of MAPS analyzed moisture and temperature fields for verification, the fit of these fields to surface observations (rms difference of less than 10% for RH and approximately 1 K for temperature) is somewhat less than the rms forecast errors. Finally, it should also be mentioned that the 2LAD, 3LAD, and PM schemes use different formulations for the stability dependence of the surface exchange coefficients. The effects of this difference were examined using the 1D model and found to be insignificant.

b. Comparison of the Blackadar and Mellor–Yamada schemes

In this section, we compare 3D simulation results between the MY and BL for the 6-day period from 23 to 28 May 1993. For the MY scheme, mean error fields at the fifth model level (not shown) indicate a cold bias over most areas. The largest errors are over the Rocky Mountain areas and southwest areas of the domain. Over lower-terrain areas in the central and eastern United States, errors are quite small. The mean errors from the BL scheme are quite similar to those from the MY scheme over the western United States but the cold bias is somewhat larger over the eastern United States. On the other hand, the BL scheme has a significant warm bias in surface temperature forecasts, whereas the MY scheme shows a slight cold bias for the same field (figure not shown). For moisture prediction, both schemes produce positive mean errors in relative humidity but those of the BL scheme are larger, especially in the mountainous western United States.

Root-mean-square relative humidity and temperature errors for the BL and MY 3D experiments over the 6-day test are shown in Table 4b. These rms errors are considerably reduced using the MY scheme compared to results from the BL scheme for both relative humidity and temperature. The improvement from the MY scheme is more pronounced at the surface than at levels 3 and 5.

7. Conclusions and discussion

This study compares several formulations parameterizing the surface latent heat flux and boundary-layer processes with 1D and 3D models. The 3D model used is the isentropic-sigma hybrid model that is part of MAPS developed at the National Oceanic and Atmospheric Administration/Environmental Research Laboratory/Forecast Systems Laboratory, and the 1D model is extracted from the 3D model. Several case studies and quasi real-time forecasts were made.

A modified formula for computing the surface moisture flux is proposed based on the assumption that the layer below the lowest model computational level can be represented by three "physical" layers, of which the bottom one is the molecular layer. This 3LAD scheme is compared with 2LAD as well as RS and PM schemes. Both an ensemble of ten 12-h forecasts (3D) and case simulations (1D) demonstrate that the 3LAD scheme produces the best prediction of latent heat flux from the ground, the mixing ratio in the atmosphere, and (for the 3D ensemble test) smaller rms differences between forecasts and verifying analyses. The 2LAD scheme produces a surface moisture flux that is too large and a boundary layer that is too moist, especially over warm and moist surfaces. The performance of the PM scheme was between that of the 2LAD and 3LAD schemes. The 12-h 3D forecast rms differences in relative humidity using the 3LAD, PM, and 2LAD schemes near the surface (10 m AGL) were 15.6%, 21.5%, and 26.0%, respectively. The rms errors in temperature among the 3LAD, 2LAD, and PM schemes were very similar at about 4 K. The performance of the RS scheme in 1D tests was close to that of the PM scheme.

The aerodynamic formula often overestimates the moisture flux from the ground in mesoscale models (Nappo 1975; Zhang and Anthes 1982) and in global-scale models (Pan 1990). This result is also shown in our 2LAD results. However, we find that the procedure for incorporating the aerodynamic formula is important, too. The one-layer formula, where the contribution from molecular diffusion is totally ignored, should give very large errors, although we did not test it in this paper. The 2LAD scheme considers partially the effects

of molecular diffusion but it still substantially overpredicts the moisture from the ground. However, with the 3LAD concept, the aerodynamic formula no longer overpredicts the moisture flux compared to the PM scheme.

It should be noted that the performance of the 3LAD scheme is dependent on the choice for the molecular layer thickness Z_μ. In this paper, the thickness of the molecular layer Z_μ is assumed to be inversely proportional to the turbulent momentum flux at the lowest model level (10 m) under the premise that the more turbulent the atmosphere near the ground, the thinner will be the layer dominated by molecular diffusion. However, determination of the appropriate thickness for the molecular layer warrants further investigation.

In our study, the 3D experiments show that the PM scheme predicts much less moisture flux than the 2LAD scheme, avoiding the 2LAD's systematic overprediction of surface moisture flux. This result is in agreement with that obtained from the global-scale model (Pan 1990).

We also compared the parameterizations of vertical turbulent transport by Blackadar and Mellor–Yamada (level 2.0). The 1D tests show that under conditions of strong surface heating, the MY scheme produces more downward heat flux through the top of the mixed layer than the BL scheme when the static stability in the free atmosphere above the mixed layer is appreciable, resulting in a warmer mixed layer. This difference between the two schemes is much less when the free atmosphere has low static stability. The 3D comparisons demonstrate that, for the cases run, the MY scheme produces smaller forecast errors than the BL scheme.

The temporal variation of the turbulent exchange coefficient implied by the BL scheme is greater than that computed by the MY scheme. Discontinuities in implied turbulence were associated with transitions between different stability regimes, especially those from the forced turbulence to the free convection regime in the morning, or vice versa in the late afternoon.

Previous studies (e.g., Mesinger and Lobocki 1991) have shown that the more complicated MY 2.5 and 3.0 schemes are very effective. Our study demonstrates that even the level 2.0 scheme is also very effective and superior to the BL scheme for the cases run. The level 2.5 or higher schemes require prediction of turbulence variables—a time-consuming process. All levels of the MY scheme require the computation of a master length l, which involves an empirical constant α that is taken as 0.1 in most applications. In our application, the turbulent exchange coefficient K_h is almost proportional to α^2. Mellor and Yamada (1974) tested $\alpha = 0.05$, and the result seemed to be not as good as for $\alpha = 0.1$. In our case, however, $\alpha = 0.05$ gave a more realistic turbulent exchange coefficient value than $\alpha = 0.1$, although K_h still sometimes exceeds 100 $m^2 s^{-1}$, which is considered a large value. The reason $\alpha = 0.05$ produces more realistic results may relate to the coarse vertical resolution in our model tests so that the maximum in the kinetic energy profile may not be as well captured as in their models. We have seen that even $\alpha = 0.05$ produces strong vertical mixing under convective conditions. Thus, when running forecast models with low vertical resolution, the empirical constant α used for calculating l_0 may need to be smaller than that used in high-resolution boundary-layer models.

Finally, it should be mentioned that, in reality, the moisture flux from the ground is a combination of bare-soil direct evaporation and plant canopy evaporation and transpiration. It depends on soil type, vegetation, and many other factors. Since this study is oriented toward an operational forecast model, we have used a relatively simple parameterization. A multilayer soil model with reasonably sophisticated vegetation treatment will be tested with the next generation of the MAPS model.

Acknowledgments. The authors are deeply indebted to Dr. Thomas Schlatter for consistent encouragement and support for this study. We are very grateful to Prof. Rainer Bleck for his contribution to writing the Mellor–Yamada 2.0 code. Also, the authors would like to thank Ms. Tracy L. Smith and other members of the MAPS group for their constant assistance in MAPS coding. We would like to thank Dr. Everett Nickerson for his careful review, and Dr. Hua-Lu Pan for his insightful suggestions. Finally, we are grateful to Ms. Chris Thomas and Ms. Nita Fullerton for their careful editing. This study is partially supported by the FAA Aviation project at FSL.

APPENDIX A

List of Main Symbols

c_g	thermal capacity of a slab per unit ground area
c_p	specific heat capacity of air at constant pressure
C_q	surface exchange coefficient (dimensionless)
D	boundary-layer depth
e	entrainment coefficient (0.2)
E_a	air moisture deficit
E_p, E	potential and actual evapotranspiration
f	Coriolis parameter
g	gravitational acceleration
G	heat flux into the ground
H	sensible heat flux from ground
H_a	sensible heat flux at the top of the surface layer for the Blackadar scheme
k	von Kármán constant (0.4)
K_m, K_h	turbulent exchange coefficients for momentum and heat

K_q turbulent mixing coefficient
K_{z0} background exchange coefficient (= 1.0 $m^2 s^{-1}$)
l master length in the Mellor–Yamada scheme
L Monin–Obukhov length
$L\downarrow$ longwave radiation incident on the surface
l_k constant mixing length (= 400 m)
L_v specific heat of evaporation
M soil moisture availability
q square root of turbulence kinetic energy
q_{gs}, q_s saturated mixing ratio at the ground surface and in the air
q_v air mixing ratio at the surface
R_f, Ri, Ri_c flux, gradient, and critical (0.2) Richardson numbers
R_n net radiation
r_s surface stomatal resistance (60 s m^{-1})
S_h, S_m stability parameters for heat and momentum in the Mellor–Yamada scheme
$S\downarrow$ shortwave radiation incident on the surface
T_a, T_g temperature at the lowest model level and ground
u, v, U_g, V_g x, y components of horizontal wind and geostrophic wind
u_* friction velocity
V_a surface wind speed at lowest model level
w weighting function of airmass mixing in Blackadar scheme
W_g volumetric moisture concentration of soil (dimensionless)
$W_{\max}$ maximum volumetric moisture concentration of soil [dimensionless, = 0.4 for sandy clay (Wetzel and Chang 1987)]
Z_0 surface roughness height
Z_a height at the lowest model level (10 m)
Z_l (0.01 m over land and Z_0 over water)
Z_μ depth of the molecular layer
α constant for master length in the Mellor–Yamada level 2.0 scheme (0.05)
α_i generic variable at level i
β surface albedo
ϵ surface emissivity
θ_{va}, θ_v virtual potential temperature at lowest and other model levels
ν_q molecular diffusivity for water vapor (= 2.4×10^{-5} $m^2 s^{-1}$)
ρ_a, ρ air density at the lowest and other model levels
ϕ_h, ϕ_m, ϕ_q nondimensional vertical gradient for heat, momentum, and water vapor
ψ_h, ψ_m stability correction term for heat and momentum
σ Stefan–Boltzmann constant, vertical coordinate

APPENDIX B

Equations for Mellor–Yamada Level 2.0 Scheme

The turbulence exchange coefficients for momentum and heat in Mellor–Yamada level 2.0 closure are calculated as follows (see appendix A for a list of symbols):

$$K_m = l^2\left\{\left[\left(\frac{\partial u}{\partial z}\right)^2 + \left(\frac{\partial v}{\partial z}\right)^2\right][B_1(1 - R_f)S_M]\right\}^{1/2} S_M, \tag{B1}$$

$$K_h = l^2\left\{\left[\left(\frac{\partial u}{\partial z}\right)^2 + \left(\frac{\partial v}{\partial z}\right)^2\right][B_1(1 - R_f)S_M]\right\}^{1/2} S_H, \tag{B2}$$

where

$$S_M = \frac{(F_3 - F_4 R_f)}{(F_5 - F_6 R_f)} S_H, \tag{B3}$$

$$S_H = \frac{(F_1 - F_2 R_f)}{(1 - R_f)}, \tag{B4}$$

$$R_f = \left(\frac{S_H}{S_M}\right)\mathrm{Ri}. \tag{B5}$$

Parameters F_1 through F_6 are derived from the constants A_1, A_2, B_1, B_2, and C_1 in Mellor and Yamada (1982, designated as MY82) and are expressed as follows:

$$F_1 = 3A_2\gamma_1,$$
$$F_2 = 3A_2(\gamma_1 + \gamma_2),$$
$$F_3 = A_1B_1(\gamma_1 - C_1),$$
$$F_4 = A_1[B_1(\gamma_1 - C_1) + 6A_1 + 3A_2],$$
$$F_5 = A_2B_1\gamma_1,$$
$$F_6 = A_2[B_1(\gamma_1 + \gamma_2) - 3A_1].$$

Note that in the expression for F_4 a minor error in MY82 has been corrected (Lobocki 1992). Moreover,

$$\gamma_1 = \frac{1}{3} - \frac{2A_1}{B_1},$$

$$\gamma_2 = \frac{(B_2 + 6A_1)}{B_1},$$

and (A_1, A_2, B_1, B_2, C_1) = (0.92, 0.74, 16.6, 10.1, 0.08).

REFERENCES

Anthes, R. A., E.-Y. Hsie, and Y.-H. Kuo, 1987: Description of the Penn State/NCAR Mesoscale Model Version 4 (MM4). NCAR Tech. Note, NCAR/TN-282+STR, 66 pp.

Argentini, S., P. J. Wetzel, and V. M. Karyampudi, 1992: Testing a detailed biophysical parameterization for land–air exchange in

a high-resolution boundary-layer model. *J. Appl. Meteor.*, **31,** 142–156.

Benjamin, S. G., and T. N. Carlson, 1986: Some effects of surface heating and topography on the regional severe storm environment. Part I: Three-dimensional simulations. *Mon. Wea. Rev.*, **114,** 307–329.

——, T. L. Smith, P. A. Miller, D. Kim, T. W. Schlatter, and R. Bleck, 1991: Recent improvements in the MAPS isentropic-sigma data assimilation system. Preprints, *Ninth Conf. on Numerical Weather Prediction,* Denver, CO, Amer. Meteor. Soc., 118–121.

——, R. Bleck, G. Grell, Z. Pan, T. L. Smith, J. M. Brown, J. E. Ramer, P. A. Miller, and K. A. Brundage, 1993: Aviation forecasts from the hybrid-b version of MAPS—Effects of a new vertical coordinate and improved model physics. Preprints, *Fifth Conf. on Aviation Weather Systems,* Vienna, VA, Amer. Meteor. Soc., J5–J9.

Blackadar, A. K., 1976: Modeling the nocturnal boundary layer. Preprints, *Third Symp. on Atmospheric Turbulence, Diffusion and Air Quality.* Raleigh, NC, Amer. Meteor. Soc., 46–49.

——, 1979: Modeling pollutant transfer during daytime convection. Preprints, *Fourth Symp. on Turbulence, Diffusion and Air Pollution.* Reno, NV, Amer. Meteor. Soc., 443–447.

Bleck, R., and S. G. Benjamin, 1993: Regional weather prediction with a model combining terrain-following and isentropic coordinates. Part I: model description. *Mon. Wea. Rev.*, **121,** 1770–1785.

Carlson, T. N., and F. E. Boland, 1978: Analysis of urban–rural canopy using a surface flux heat/temperature model. *J. Appl. Meteor.*, **17,** 998–1013.

Charney, J. G., W. J. Quirk, S. H. Chow, and J. Kornfield, 1977: A comparative study of the effects of albedo change on drought in semi-arid regions. *J. Atmos. Sci.*, **34,** 1366–1385.

Clarke, R. H., A. J. Dyer, R. R. Brook, D. G. Reid, and A. J. Troup, 1971: The Wangara experiment: Boundary layer data. Tech. Paper No. 19, Division of Meteorological Physics, CSIRO, Australia 363 pp.

Davies, J. A., and C. D. Allen, 1973: Equilibrium, potential and actual evaporation from cropped surfaces in southern Ontario. *J. Appl. Meteor.*, **12,** 649–657.

Deardorff, J. W., 1972: Parameterization of the planetary boundary layer for use in general circulation models. *Mon. Wea. Rev.*, **100,** 93–106.

——, 1978: Efficient prediction of ground surface temperature and moisture with inclusion of a layer of vegetation. *J. Geophys. Res.*, **93,** 1889–1903.

Grell, G. A., 1993: Prognostic evaluation of assumptions used by cumulus parameterizations. *Mon. Wea. Rev.*, **121,** 764–787.

Janjic, Z. I., 1990: The step-mountain coordinate: Physical package. *Mon. Wea. Rev.*, **118,** 1429–1443.

Lettau, H. H., and B. Davidson, 1957: *Exploring the Atmosphere's First Mile.* Vols. I and II. Pergamon Press, 578 pp.

Lobocki, L., 1992: Mellor–Yamada simplified second-order closure models: Analysis and application of the generalized von Karman local similarity hypothesis. *Bound.-Layer Meteor.*, **59,** 83–109.

Manabe, S., J. Smagorinsky, and R. F. Strickler, 1965: Simulated climatology of a general circulation model with a hydrological cycle. *Mon. Wea. Rev.*, **93,** 769–798.

Mahrt, L., and M. Ek, 1984: The influence of atmospheric stability on potential evaporation. *J. Climate Appl. Meteor.*, **23,** 222–234.

Mellor, G. L., 1982: Development of a turbulence closure model for geophysical problems. *Rev. Geophys.*, **20,** 851–875.

——, and T. Yamada, 1974: A hierarchy of turbulence closure models for planetary boundary layers. *J. Atmos. Sci.*, **31,** 1791–1806.

Mesinger, F., and L. Lobocki, 1991: Sensitivity to the parameterization of surface fluxes in NMC's eta model. Preprints, *Ninth Conf. on Numerical Weather Prediction,* Denver, CO, Amer. Meteor. Soc., 213–216.

Miyakoda, K., and J. Sirutis, 1977: Comparative integrations of global models with various parameterized processes of subgrid-scale vertical transports: Description of the parameterizations. *Beitr. Phys. Atmos.*, **50,** 445–487.

Monteith, J. L., 1965: Evaporation and environment. *Symp. Soc. Exp. Biol.*, **XIX,** 205–234.

Nappo, C. J., 1975: Parameterization of surface moisture and evaporation rate in a planetary boundary layer model. *J. Appl. Meteor.*, **14,** 289–296.

Pan, H.-L., 1990: A simple parameterization scheme of evapotranspiration over land for the NMC medium-range forecast model. *Mon. Wea. Rev.*, **118,** 2500–2512.

Penman, H. L., 1948: Natural evaporation from open water, bare soil and grass. *Proc. Roy. Soc. London,* **A193,** 120–145.

Raymond, W. H., and R. B. Stull, 1990: Application of transilient turbulence theory to mesoscale numerical weather forecasting. *Mon. Wea. Rev.*, **118,** 2471–2499.

Segal, M., G. Kallos, J. Brown, and M. Mandel, 1992: Morning temporal variations of shelter-level specific humidity. *J. Appl. Meteor.*, **31,** 74–85.

Stull, R. B., 1988: *An Introduction to Boundary Layer Meteorology.* Kluwer Academic Publishers, 274 pp.

——, 1991: Static stability—An update. *Bull. Amer. Meteor. Soc.*, **72,** 1521–1529.

Wetzel, P. J., and J.-T. Chang, 1987: Concerning the relationship between evapotranspiration and soil moisture. *J. Climate Appl. Meteor.*, **26,** 18–26.

Yamada, Y., and G. L. Mellor, 1975: A simulation of the Wangara atmospheric boundary layer data. *J. Atmos. Sci.*, **32,** 2309–2329.

Zhang, D.-L., and R. A. Anthes, 1982: A high-resolution model of the planetary boundary layer—Sensitivity tests and comparisons with SESAME-79 data. *J. Appl. Meteor.*, **21,** 1594–1609.